A Pixelated MIMO Wireless Optical Communication System

Steve Hranilovic, *Member, IEEE*, and Frank R. Kschischang, *Fellow, IEEE*

Abstract—This paper introduces the *pixelated wireless optical channel*, which transmits data at high rates using a series of coded time-varying images. This multiple-input/multiple-output point-to-point wireless optical channel uses arrays of optical intensity transmitters and detectors to exploit the inherent spatial degrees of freedom and to realize significant gains in spectral efficiency over single-element systems. Spatial discrete multitone modulation is introduced as a means to combat low-pass spatial distortion and to alleviate spatial alignment problems of previous systems. The capacity of pixelated wireless optical channels is estimated by way of a water-pouring spectrum. A proof-of-concept experimental prototype is constructed using a 512×512 pixel liquid crystal display panel and 154×154 pixels of a charge-coupled device camera. A channel model is developed and the capacity estimated to be 22.4 kb/frame. An unoptimized multilevel code and multistage decoder is applied over the spatial frequency bins and shown to yield spectral efficiencies of approximately 1.7 kb/s/Hz over a range of 2 m.

Index Terms—Multiple-input/multiple-output (MIMO) wireless optical channel, optical intensity modulation, optical space–time code, short-range wireless infrared channel, spatial modulation and coding.

I. INTRODUCTION

IT is often said that "a picture is worth a thousand words," and in this paper we use this concept to create a high-rate wireless optical communication channel, termed the *pixelated wireless optical channel*. The basic idea is very simple [1]–[3]: We use a two-dimensional (2-D) array of optical transmitters to form a sequence of coded images (such as, e.g., the image shown in Fig. 1), which are detected by an imaging receiver. For short-range links, where the signal-to-noise ratio (SNR) is large enough, we are able to achieve large gains in spectral efficiency over single-element links. The purpose of this paper is: 1) to introduce a framework for the design of spatio-temporal coding in pixelated wireless optical channels; 2) to estimate the information theoretic capacity of such channels; 3) to introduce an experimental prototype; and 4) to quantify the potential per-formance that can be achieved in the prototype channel with practical encoding and decoding complexity.

There are a number of potential applications for systems of this type. For example, low-cost cameras are being included in a wide variety of consumer products such as cellphones and PDAs; we envision that, in addition to their primary purpose, these cameras might be used as short-range high-speed digital communication ports, providing a secure link free of mechanical wear and interface issues. We are not the first to consider using multiple optical transmitters and receivers to realize a gain; indeed, for the purpose of connecting circuit boards to a high-speed optical backplane, optical interconnect systems with hundreds of parallel noninteracting channels have been considered [4]–[10]. An important practical difficulty with such systems is that precise spatial alignment between transmitter and receiver is necessary in order to avoid interchannel interference (ICI). The approach taken in this paper is a generalization of this previous work in that ICI is specifically modeled and accounted for in the coding and signal design, making precise spatial alignment unnecessary. The techniques developed in this paper, may also be useful to ease strict spatial alignment requirements in holographic storage systems [11]. The incoherent pixelated wireless optical channel, considered in this work, is appropriate for point-to-point high-speed short-range communications for the purposes of data interchange for backplane interconnect. Due to its limited range and requirement for a line-of-sight, this link is a high rate complement, rather than replacement, to present-day mobile radio links.

Previous works in the area of point-to-point (as opposed to diffuse; see, e.g., [12], [13]) optical links used single-element transmitters and receivers. Important examples are the standard Infrared Data Association (IrDA)[1] links that operate over 1 m at rates of 4 Mb/s, as well as experimental tracked line-of-sight links operating at rates approaching a gigabit per second [14]. The primary limitation on the frequency response of such links is the photodiode depletion capacitance that arises due to the use of large, inexpensive photodiodes which are operated with limited reverse bias. In IrDA systems, the bandwidth of the receiver is in the range of 10–12 MHz, which is at least three orders of magnitude smaller than fiber optic systems. As a result, spectrally efficient modulation techniques have been considered to improve data rates on wireless optical channels [15]–[21]. The use of multiple optical transmitters has previously been considered in a variety of wireless optical links. Multielement diffuse and quasi-diffuse wireless optical links using discrete [22], [23] and imaging [24]–[26] receivers,

S. Hranilovic is with the Department of Electrical and Computer Engineering, McMaster University, Hamilton, ON L8S 4K1, Canada (e-mail: hranilovic@mcmaster.ca).

F. R. Kschischang is with the Department of Electrical and Computer Engineering, University of Toronto, Toronto, ON M5S 3G4, Canada (e-mail: frank@comm.utoronto.ca).

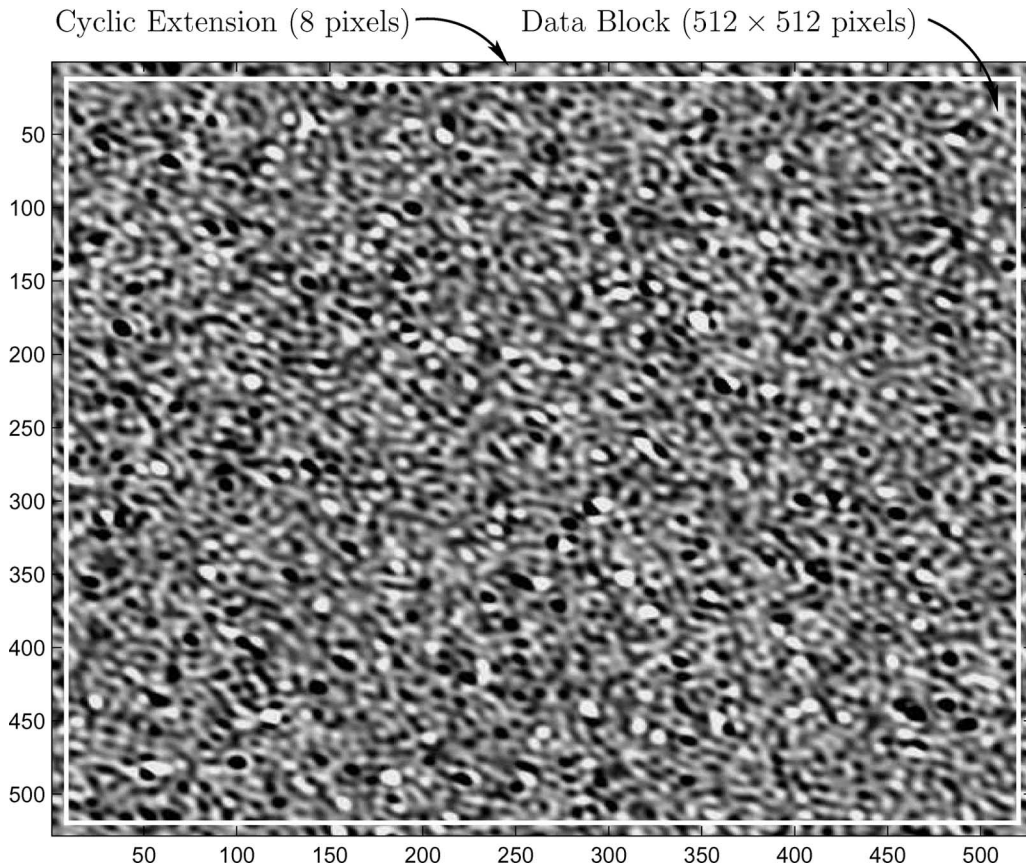[1] Infrared Data Association. [Online]. Available: http://www.irda.org

Fig. 1.   SDMT symbol with cyclic extension.

and a variety of combining and coding schemes [27], [28] have been considered to achieve gains in optical power efficiency. However, in previous work, identical optical signals are transmitted in all spatial directions (equivalent to a spatial repetition code), yielding no improvements in spectral efficiency. Multi-element links have also been proposed for long-range wireless optical channels to mitigate the impact of fading [29]. These channels differ significantly from short-range links (which do not exhibit fading) and are therefore not considered in this work.

There is a close connection between this paper and multiple-input/multiple-output (MIMO) systems at radio frequencies (RF). Whereas, current RF MIMO systems have been proposed with as many as 16 transmitter or receiver antennas, here, we consider systems using on the order of 10^5 transmit elements and 10^4 receive elements. These provide a large number of degrees of freedom, over which the power constraint is spread, enabling large multiplexing gains to be achieved. Unlike RF MIMO systems, the use of spatial diversity to mitigate fading is not an issue in the short-range optical links considered here.

The remainder of this paper is organized as follows. Section II provides a mathematical model for the pixelated wireless optical channel and justifies the assumptions made. A simple experimental prototype system is presented along with channel measurements to justify the derived channel model. The reader familiar with the modeling of imaging systems can take the channel model in (8) and proceed to Section III, which discusses the fundamental information theoretic limits to data transmission on

this MIMO optical channel. The channel capacity of MIMO pixelated wireless optical channels is estimated in the general case as well as for the prototype channel. Practical spatio-temporal modulation and coding techniques to approach the channel capacity are presented in Section IV along with an algorithm for spatial synchronization. Section V presents concluding remarks and directions for future work.

II. MIMO WIRELESS OPTICAL CHANNEL

We consider links that use inexpensive optical intensity modulators, such as light-emitting diodes (LEDs), whose output intensity varies in response to an electrical signal. Since only the intensity can be modulated, all transmitted electrical signals are restricted to nonnegative values. Additionally, the average optical power transmitted, i.e., the average amplitude, is limited due to skin- and eye-safety considerations. The optical direct detection receiver elements output an electrical photocurrent proportional to the received optical intensity.

The propagation characteristics of this short-range wireless channel differ from conventional radio frequency wireless channels due to the lack of multipath fading. The receiver photodiode integrates the optical intensity field over an area of millions of square wavelengths providing a degree of inherent spatial diversity [30], [13].

In this section, we present a discussion on the basic structure of the pixelated wireless optical channel as well as mathematical models for deterministic and stochastic channel impairments.
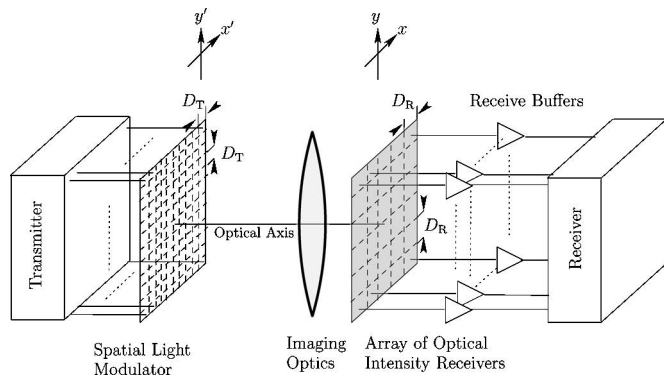
Fig. 2. Block diagram of the pixelated wireless optical channel.

A. Channel Configuration

Fig. 2 presents a block diagram of a pixelated wireless optical channel.

The transmitter is a *spatial light modulator* (SLM), which produces an output optical intensity spatial distribution controlled by electrical addressing [31]. Examples of transmit arrays include liquid crystal displays (LCDs), arrays of LEDs or vertical cavity surface emitting lasers (VCSELs), organic polymer LEDs (OLEDs) as well as deformable micro-mirror devices (DMDs) (when coupled with projection optics).

The receiver is oriented to capture the transmitted image and produces an output electrical signal representing the spatial distribution of optical power impinging on the device. Typical examples of such receivers are charge-coupled device (CCD) cameras, CMOS imagers as well as arrays of photodiodes. Appropriate optics are employed to form a focused image on the surface of the detector array.

We assume that the transmitter and receiver locations are fixed and that the channel characteristics are stationary in time. This situation is realistic in the case of backplane applications or in situations in which the channel varies slowly and can be tracked. Furthermore, it is assumed that the optical axes of the transmitter and the receiver are aligned. In this on-axis configuration, the receive image is an *orthographic projection* of the transmitted image and there is no perspective distortion [32]. The orthographic projection assumption is valid for optical backplane and holographic storage applications. In many cases, this assumption is nearly true or it can be corrected by spatial predistortion techniques. Commercial video-processing equipment exists that removes projective distortion in the case of off-axis projection [33].

In this paper, we consider the case of both transmit and receive pixels spaced on the 2-D integer lattice. Many optical systems have point-spread functions with circular symmetry due to the shape of their apertures. 2-D signals that are bandlimited over a circular region in spatial frequency domain are optimally sampled using a hexagonal lattice in the sense of reducing the number of samples required to represent the images [34]. In fact, a saving of over 13% fewer samples can be realized by using optimum hexagonal sampling over rectangular [35]. Although small hexagonally spaced arrays have been considered

for diversity detection in turbulent free-space optical links [36], a vast majority of commercial SLMs and receiver arrays have elements arranged on rectangular grids.

In this paper, we assume that incoherent intensity modulation and direct detection are employed at the transmitter and receiver arrays, respectively. We focus on these types of links due to their lower cost, improved eye and skin safety properties, and simpler implementation. It is possible to consider a coherent MIMO wireless optical channel consisting of arrays of coherent transmitters and wavefront sensors. Fundamentally, coherent systems allow for the modulation and detection of the wavefront directly and permit more flexible spatial filtering options. However, the cost and complexity of such systems make them currently impractical, and thus, they are not treated in this paper. In the remainder of this paper, all signals are assumed to be spatial optical intensity distributions, and are thus restricted to nonnegative amplitudes. Additionally, although we consider the case in which images are formed by intensity modulating a single band of wavelengths, i.e., a single color, it is also possible to consider using multicolor images. Multiwavelength transmitters and receivers provide an additional degree of freedom in code design and can be used to realize a multiplexing gain. However, it should be noted that, in general, the point-spread function, defined in the next section, is wavelength-dependent.

The key differences between our definition of the pixelated MIMO channel and previously proposed MIMO optical backplanes is that strict spatial alignment of the receiver and transmitter pixels is not required, nor does the resolution of the transmitter and receiver arrays need to be identical. Here, we only assume that the transmitter is in the field-of-view of the receiver. The receiver determines the mapping between the camera coordinates and those of the transmit array in a process termed *spatial registration*. In machine vision applications, spatial registration is performed during camera calibration [32] and is accomplished with the aid of calibration markers, termed *fiducials*, known *a priori* at the receiver. The design of fiducials which allow for sub-pixel alignment accuracy has been investigated [37]. It must be noted, however, that although the receiver can determine the position of the transmit pixels in the field-of-view, it is not possible to adjust the phase or frequency of the spatial sampling since these parameters are determined by the pixel size of the imager and the separation of transmitter and receiver. Section IV-B presents a solution to the spatial synchronization problem in the case of spatial discrete multitone (SDMT) modulation.

B. Mathematical Model: Deterministic Distortion

Denote $i_T(x', y'; t)$ as the emitted spatial optical intensity distribution on the transmitter plane and $i_R(x, y; t)$ as the received spatial distribution of optical intensity over the imager plane both at time t, as shown in Fig. 2.

Let M denote the magnification predicted by geometrical optics of the imaging system from the transmitter plane to the imager plane and define $i_T'(x, y; t)$ as the image of the transmitted image on the imager plane due solely to geometric

optics, namely

$$\mathsf{i}'_{\mathrm{T}}(x, y; t) = \frac{1}{|M|} \mathsf{i}_{\mathrm{T}}(x/M, y/M; t). \tag{1}$$

Under these conditions and the assumption of narrowband illumination, this imaging system can be well modeled as linear and spatially invariant in terms of optical intensity [38, Sec. 6.3].

Let $h(x, y)$ denote the *point-spread function* characterizing the response of this imaging system to a spatial impulse of optical intensity. Fundamentally, $h(x, y)$ is limited by diffraction due to the finite aperture size of practical components [38]; however, it is typically dominated by implementation effects which will be discussed shortly. The use of a linear spatially invariant filtering operation to model optical imaging systems is a popular and well established technique [38, Ch. 6]. Thus, in the absence of noise, the spatial distribution of intensity at the receiver, $\mathsf{i}_{\mathrm{R}}(x, y; t)$, can be related to the transmitted intensity image via

$$\mathsf{i}_{\mathrm{R}}(x, y; t) = \int_{-\infty}^{\infty} \int_{-\infty}^{\infty} h(x - \bar{x}, y - \bar{y}) \mathsf{i}'_{\mathrm{T}}(\bar{x}, \bar{y}; t) d\bar{x}\, d\bar{y}$$
$$= h \otimes \mathsf{i}'_{\mathrm{T}}(x, y; t) \tag{2}$$

where $\otimes$ is the 2-D convolution operator.

Most practical SLMs are able to produce an output optical intensity distribution that is discretized in both space and time. We assume that the transmitter consists of n_{T} identically shaped transmit pixels spaced at intervals of D_{T} on a square grid of size $n_{\mathrm{T}x} \times n_{\mathrm{T}y}$ in each spatial coordinate. Define $p_{\mathrm{T}}(x', y')$ as the transmit pixel *aperture function* that represents the spatial optical intensity distribution for each transmit pixel. We additionally assume that for some period T seconds, if $t \in [iT, (i + 1)T)$ then $\mathsf{i}_{\mathrm{T}}(x', y'; t) = \mathsf{i}_{\mathrm{T}}(x', y'; iT)$, i.e., each pixel transmits a rectangular pulse amplitude-modulated (PAM) signal with symbol interval T. At each symbol period, iT, a data-bearing transmit image is formed by defining a matrix of $n_{\mathrm{T}x} \times n_{\mathrm{T}y}$ real, nonnegative values, $a[m, n; iT] \geq 0$, to modulated each pixel. The resulting transmitted optical intensity image at time iT, for $i \in \mathbb{Z}$, is defined as

$$\mathsf{i}'_{\mathrm{T}}(x, y; iT)$$
$$= \sum_{m=0, n=0}^{n_{\mathrm{T}x}-1, n_{\mathrm{T}y}-1} a[m, n; iT] p'_{\mathrm{T}}(x - mD'_{\mathrm{T}}, y' - nD'_{\mathrm{T}}).$$

Using (1), with reference to the image plane,

$$\mathsf{i}'_{\mathrm{T}}(x, y; iT)$$
$$= \sum_{m=0, n=0}^{n_{\mathrm{T}x}-1, n_{\mathrm{T}y}-1} a[m, n; iT] p'_{\mathrm{T}}(x - mD'_{\mathrm{T}}, y' - nD'_{\mathrm{T}})$$

where $D'_{\mathrm{T}} = D_{\mathrm{T}}/M$ and $p_{\mathrm{T}}'(x, y) = 1/|M| p_{\mathrm{T}}(x/M, y/M)$. Thus, the intensity at the imager plane can be written using (2)

as

$$\mathsf{i}_{\mathrm{R}}(x, y; iT) = \sum_{m=0, n=0}^{n_{\mathrm{T}x}-1, n_{\mathrm{T}y}-1} a[m, n; iT]$$
$$h \otimes p'_{\mathrm{T}}(x - mD'_{\mathrm{T}}, y - nD'_{\mathrm{T}}). \tag{3}$$

Practical receivers consist of an array of photodetecting pixels, which integrate $\mathsf{i}_{\mathrm{R}}(x, y; iT)$ in time and in space, and output a sample for each pixel every T seconds. The receiver array consists of n_{R} receive pixels spaced at intervals of size D_{R} on a square grid of size $n_{\mathrm{R}x} \times n_{\mathrm{R}y}$ in each coordinate. The aperture function of each receive pixel, $p_{\mathrm{R}}(x, y)$, is assumed identical for each pixel. This function represents the extent and shape of the received pixel and accounts for any variability in the responsivity of the pixel in space. The receiver is a temporal and spatial optical intensity sampler and at each symbol interval outputs the $n_{\mathrm{R}x} \times n_{\mathrm{R}y}$ array $r[k, l; iT]$, which represents the sampled output of a spatial integrator in each pixel, namely

$$r[k, l; iT] = \int_{iT}^{(i+1)T} \int_{-\infty}^{\infty} \int_{-\infty}^{\infty} \mathsf{i}_{\mathrm{R}}(x, y; iT)$$
$$p_{\mathrm{R}}(x - kD_{\mathrm{R}}, y - lD_{\mathrm{R}}) dx\, dy\, dt. \tag{4}$$

Here, it is additionally assumed that the receiver and transmitter are synchronized in time and that there is no temporal intersymbol interference (ISI). Also, the propagation delay between transmitter and receiver is assumed to be constant and is ignored. Data symbol timing recovery could potentially take place by transmitting the clock on a separate spatial channel or using conventional baud-rate timing recovery techniques [39].

The integral in time in (4) can be easily removed, since in a given symbol interval the optical intensity distribution is assumed constant. Substituting (3), gives the channel model from the input data symbols to the received sampled intensity values as

$$r[k, l; iT] = \sum_{m=0, n=0}^{n_{\mathrm{T}x}-1, n_{\mathrm{T}y}-1} a[m, n; iT]$$
$$h \otimes p'_{\mathrm{T}} \otimes p'_{\mathrm{R}}(kD_{\mathrm{R}} - mD'_{\mathrm{T}}, lD_{\mathrm{R}} - nD'_{\mathrm{T}}),$$

where $p'_{\mathrm{R}}(x, y) = T p_{\mathrm{R}}(-x, -y)$. Define

$$h_{\mathrm{sys}}(x, y) = h \otimes p'_{\mathrm{T}} \otimes p'_{\mathrm{R}}(x, y) \tag{5}$$

as a composite point-spread function of the entire imaging system. Often, optical imaging systems are analyzed in frequency domain [38, Ch. 6]. The Fourier transform of $h_{\mathrm{sys}}(x, y)$, $H_{\mathrm{sys}}(u, v)$, is termed the *optical transfer function* (OTF) and represents the spatial frequency response of the imaging system.

Therefore, the input—output response of the system can then be written as

$$r[k, l; iT] = \sum_{m=0, n=0}^{n_{\mathrm{T}x}-1, n_{\mathrm{T}y}-1} a[m, n; iT]$$
$$h_{\mathrm{sys}}(kD_{\mathrm{R}} - mD'_{\mathrm{T}}, lD_{\mathrm{R}} - nD'_{\mathrm{T}}). \tag{6}$$

The system point-spread function, $h_{\mathrm{sys}}(x,y)$, arises not only due to the aperture effects discussed but also due to a host of other effects. The linear spatial filter h in (5), is often modeled as a cascade of linear spatial filters, each representing the impact of the optics, diffraction, aberrations, and carrier diffusion effects [40, Ch. 10] [41, Sec. 4.4.2]. In fact, it has been shown that treating these effects separately and representing them as a cascade of independent linear filters provides a pessimistic estimate of the spatial bandwidth of the imaging system [42]. In general, it is difficult to compute the point-spread function analytically for a given imaging system and it is often measured. In Section II-E, the point-spread function for a prototype is measured and shown to be a low-pass spatial filter.

C. Noise

The characteristics of noise sources in electronic imaging systems have been extensively studied due to their impact on image quality [40], [41], [43]–[45]. In general, noise analysis differs for each imager, however, the dominant sources of noise are due to $1/f$ "flicker" noise, shot noise from the detected optical intensity signal and dark current as well as thermal noise generated by the readout circuitry. Qualitatively, at high illumination, the dominant source of noise is due to photodiode shot noise, which is signal-dependent, while at lower background illumination, circuit noise dominates [40, Sec. 4.2]. The noise in these imagers is typically modeled as being Gaussian-distributed. This is especially true in wireless optical channels that have high-intensity background illumination, which causes the distribution of the shot noise to approach a Gaussian distribution by a central limit theory argument [13]. Thus, a general model is a 2-D Gaussian distribution with noise variance

$$\sigma^2(x,y) = \alpha i_{\mathrm{R}}(x,y) + \beta \qquad [\mathsf{A}^2] \qquad (7)$$

where the constant α quantifies the signal dependence of the noise, and β represents signal-independent components like circuit noise, dark current noise, and shot noise due to background illumination.

The variance of the noise depends on both the received signal as well as on the receive pixel area. The variance of the received shot noise is proportional to the photocurrent generated both by the receive optical intensity as well as by dark current. Neglecting dark current noise, the variance of the shot noise is proportional to the area of the receive pixel as well as the received optical intensity [40]. Indeed, in wireless optical channels that are corrupted by high-intensity background illumination, the shot-noise variance is proportional to the photodiode area [15, Sec. 3.7.3]. In CMOS active pixel sensors, the dominant source of noise at low illumination is due to circuit noise generated by readout and reset transistors [43]–[45]. This noise is commonly referred to as kTC noise and has variance, in units of A^2, is proportional to the photodiode capacitance, and thus the pixel area. Thus, the noise variance can be well modeled as being proportional to the area of each receiver pixel.

In general, the noise sources across the receiver array have differing statistics due to the nonuniform photo-response of the pix-
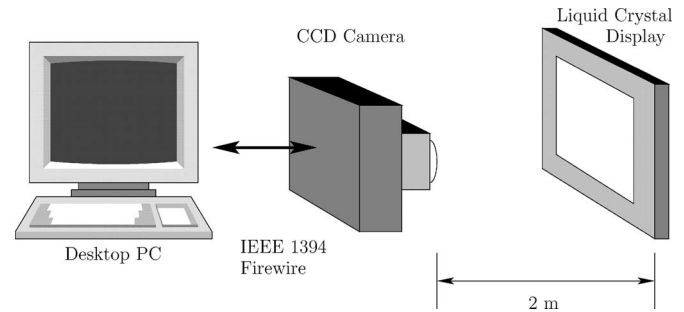

Fig. 3.   Diagram of experimental prototype.

els, commonly referred to as *fixed pattern noise*. The noise characteristics in a prototype system are measured in Section II-E.

D. Prototype Configuration

We present a simple prototype pixelated wireless optical channel, in order to measure realistic parameters for the general model presented earlier. The prototype point-to-point link is shown in Fig. 3 [46]. The transmit array consists of the LCD panel of a laptop computer with 1024×768 pixels at a dot pitch of 0.24 mm (Versa 6050MX).[2] The computer was used to interface to the display and generate 8-b gray-scale images. All transmitted images were quantized to one of the possible 256 intensity levels available to the LCD panel. The receive array was implemented using a CCD camera with a resolution of 640×480 pixels of size 10 μm $\times$ 10 μm (A301f).[3] This camera operates at 60 frames/s and outputs an uncompressed 8-b gray-scale value for each pixel. Similar to the transmitter, all received pixels are quantized to one of the available 256 levels. The transmit and receive arrays were separated by a distance of 2 m and their optical axes were approximately aligned so that the orthographic assumption was valid. There was no relative motion between the ends of the link. The lens, with focal length 25 mm, was focused on the LCD panel and the aperture was set to $f/1.6$ for all measurements to minimize detector saturation. Although most short-range links operate in the near infrared band ($\lambda = 850$–950 nm), this visible band experimental channel illustrates similar design challenges while satisfying eye-safety constraints.

This prototype configuration was chosen due to its low cost and ease of assembly. Although this is not the only implementation of a pixelated wireless optical link, it serves as a vehicle to perform channel measurements to arrive at a realistic channel model, as presented in the following section.

E. Measured Channel Parameters

A transmitted image was formed using $n_{\mathrm{T}x} = n_{\mathrm{T}y} = 512$ pixels centered in the middle of the LCD panel with all other pixels turned off. The transmitted image is quantized to one of the 256 intensity levels available. At the receiver, the corresponding received image was measured to be $n_{\mathrm{R}x} = n_{\mathrm{R}y} = 154$

---

[2]NEC Solutions America. [Online]. Available: http://support.neccomp.com
[3]Basler Vision Technologies. [Online]. Available: http://www.basler- vc.com
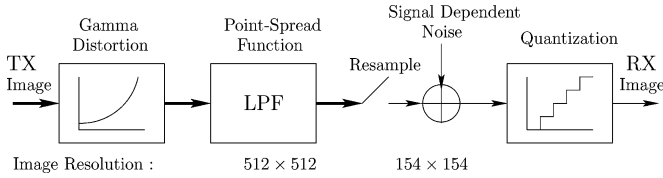
Fig. 4. Block diagram of the channel model for the point-to-point pixelated wireless optical channel.

pixels in size. Test images were transmitted to characterize the point-spread function, gamma distortion, and noise of the channel. Details of the measurement techniques and values used in the model are given in the Appendix.

The resulting channel model is presented in Fig. 4. The 512×512 transmit image is corrupted by nonlinear gamma distortion, which is present in commercial video display equipment and spatially low-pass filtered. The operation of the CCD imager is represented as a resampling of the image to a resolution of 154×154. This resampling is done by using bilinear interpolation for noninteger sampling points. Signal-dependent noise is added and the output is quantized to the 8-b levels available from the camera. A comparison between 100 transmitted binary-level images and the output of the channel model gave rise to a 5.4% error in the average energy with respect to the channel measurement. Although not insignificant, the error between the measured data is small enough to suggest that the salient properties of the channel are represented in the model and that the model is appropriate for modem-design purposes.

In this paper, it is assumed that the nonlinear gamma distortion inherent to some commercial SLMs has been compensated for using predistortion. This linearization can be done in manufacture or is programmable in some LCD SLM panels.

To summarize, using (6) and (7), the channel model for a general MIMO pixelated wireless optical channel from transmitted symbols $a[m, n; iT]$ to received array values $r[k, l; iT]$ is

$$r[k, l; iT] = n[k, l; iT]$$
$$+ \sum_{m=0, n=0}^{n_{\mathrm{T}x}-1 \, n_{\mathrm{T}y}-1} a[m, n; iT] h_{\mathrm{sys}}(kD_{\mathrm{R}} - mD'_{\mathrm{T}}, lD_{\mathrm{R}} - nD'_{\mathrm{T}}), \quad (8)$$

where $h_{\mathrm{sys}}(x, y)$ is the system point-spread function and $n[k, l; iT]$ is signal-dependent Gaussian noise with variance linearly related to the received intensity.

III. CHANNEL CAPACITY

The *capacity* of a communications channel, defined by Shannon [47], is a fundamental measure of the ability to convey information from a transmitter to a receiver. Channel capacity is the maximum rate at which reliable communication can take place, i.e., the highest rate at which we can decode the transmitted message with *any* probability of error. Shannon demonstrated that communicating at rates less than the channel capacity is a necessary and sufficient condition for reliable communication to take place.

In this section, we extend capacity results in standard models to the pixelated wireless optical channel model in (8). We show

that a fundamental parameter governing the capacity is the number of independent degrees of freedom, which are present in the channel. These degrees of freedom arise in both temporal and spatial domains. We first compute an upper bound on the channel capacity and show how it scales with the number of transmit and receive elements in a simple channel model. We then extend the analysis to arbitrary pixelated wireless optical channels and compute a capacity estimate for channels represented as (8). Practical spatial modulation and coding, which approaches these derived capacity limits are presented in Section IV.

A. Pixelated Channel Capacity: Pixel-Matched Systems

In general, the capacity of the pixelated wireless optical channel will depend on $h_{\mathrm{sys}}(x, y)$, the noise processes as well as a constraint on the average optical power, i.e., average amplitude, which can be transmitted. In this section, we treat a special case for h_{sys} and compute a tight upper bound on the channel capacity that provides insight into how the channel capacity scales with the average optical power constraint P and the number of pixels.

Consider the special case where $n = n_{\mathrm{T}} = n_{\mathrm{R}}, D'_{\mathrm{T}} = D_{\mathrm{R}}$ and

$$h_{\mathrm{sys}}(kD_{\mathrm{R}}, lD_{\mathrm{R}}) = \begin{cases} 1, & \text{if } k = l = 0 \\ 0, & \text{otherwise} \end{cases} \quad (9)$$

i.e., h_{sys} is a spatial Nyquist pulse [48]. Channels that exhibit this type of point-spread function are termed *pixel-matched*. Examples of such links include optical interconnect applications where arrays of VCSELs and photodiodes are aligned to form a large number of parallel, nearly independent wireless optical channels. The point-spread function approaches that of a spatial Nyquist pulse through the careful spatial orientation of transmit and receive arrays to ensure that emissions of each transmit pixel are received by a unique receive pixel. In this special case of the pixelated optical channel, gains in spectral efficiency are realized at the expense of alignment accuracy between the transmit and receive pixels. In the following section, we remove this alignment requirement and estimate the capacity of the pixelated channel in a more general case.

In this case of a pixel-matched h_{sys}, the channel model (8) reduces to

$$r[k, l; iT] = a[k, l; iT] + n[k, l; iT].$$

Thus, the link consists of n subchannels with no ICI. Although, the noise process is in general signal-dependent, in this example we assume that background and circuit noise dominate over the signal-dependent portion of the noise. Thus, $n[k, l; iT]$ is assumed to be identically distributed Gaussian random variables.

Let each subchannel transmit a rectangular pulse every T seconds modulated by independent M-ary PAM symbols uniformly selected from the constellation

$$\Omega = \{0, d_{\min}, \ldots, (M - 1)d_{\min}\}.$$

Notice that this signaling scheme satisfies the amplitude nonnegativity constraint. Due to the symmetry of the problem, assume that in each subchannel the average optical power limit is set

to $P_i = P/n$, where P is the limit on the total average optical power. In terms of the constellation in each subchannel [49]

$$P_i = \frac{1}{\sqrt{T}} \times \frac{M-1}{2} d_{\min}. \tag{10}$$

For an array of fixed size, increasing n implies that the area of each photodiode decreases as n. As discussed in Section II-C, to a good approximation, the noise variance for each detector depends linearly on the area of the receive pixels. Therefore, for each receive pixel $\sigma_i^2 = \sigma^2/n$, where $\sigma^2 = \sum_{i=1}^n \sigma_i^2$.

The capacity of optical intensity channels subject to non-negativity and average amplitude constraints is not known in closed form, although bounds do exist [50]. Define the centered constellation,

$$\Omega' = \begin{cases} \{0, \pm d_{\min}, \dots, \pm d_{\min}(M-1)/2\}, & M \text{ odd} \\ \{\pm d_{\min}/2, \dots, \pm d_{\min}(M-1)/2\}, & M \text{ even} \end{cases}.$$

Notice that the mutual information from input to output with uniform signaling over Ω is the same as that for Ω' [53]. At low electrical SNR, it has been shown that the capacity of the continuous additive white Gaussian noise (AWGN) channel is a tight upper bound on the mutual information of uniform signaling over Ω' [52]. It is easy to show that the average energy of Ω' in each subchannel can be written as

$$E_i = \frac{(M-1)^2}{12} d_{\min}^2 = \frac{M^2-1}{3(M-1)^2} T P_i^2$$

using (10). The SNR in each subchannel takes the form

$$\text{SNR}_i = \frac{M^2-1}{3(M-1)^2} \cdot \frac{\kappa P^2}{2W\sigma^2} \cdot \frac{1}{n} \tag{11}$$

where W is the $K\%$-fractional power bandwidth, and $\kappa = 2WT$ is the Landau–Pollak dimension of the set of signals time limited to T and with bandwidth W [53]. Since the transmitted pulse shape is time-limited, a definition for bandwidth is not obvious and a fractional power bandwidth measure is adopted here. In [49], in the case of rectangular pulses, the effective dimension was computed as $\kappa = 20.57$ with a 99%-fractional power bandwidth definition.

Thus, the capacity of the pixel-matched system is upper-bounded by

$$C \leq$$
$$C^{\text{up}} = \frac{n}{\kappa} \log\left(1 + \frac{\kappa(M^2-1)}{6(M-1)^2} \cdot \frac{P^2}{W\sigma^2} \cdot \frac{1}{n}\right)$$
$$[\text{b/s/Hz}]. \tag{12}$$

As $n \to \infty$, and defining the optical signal-to-noise ratio (OSNR) as $P/\sqrt{W\sigma^2}$

$$C^{\text{up}} \to \frac{M^2-1}{6(M-1)^2} \cdot \frac{P^2}{W\sigma^2} \cdot \frac{1}{\ln 2}$$
$$= \frac{M^2-1}{6\ln(2)(M-1)^2} \text{OSNR}^2.$$

Thus, as the number of pixels increases, the upper bound grows quadratically with the OSNR. Fig. 5 plots (12) for $M = 2$ and OSNR $= 10$ dB along with results by numerically computing the mutual information of the optical constellation for uniform
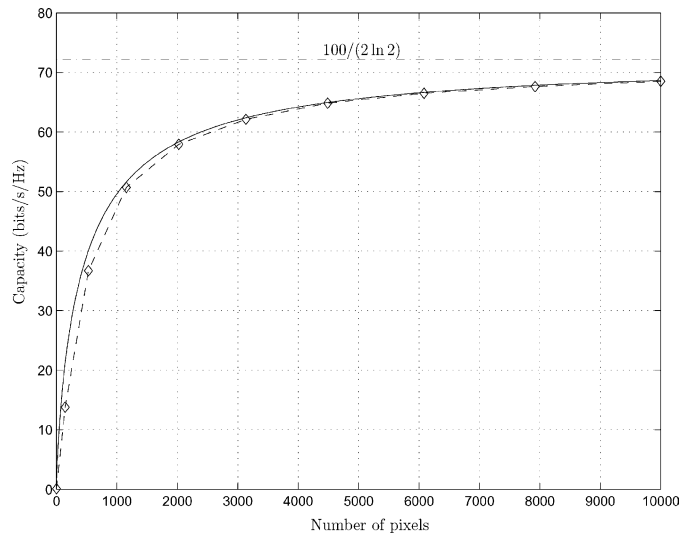

Fig. 5. Capacity [b/(s.Hz)] as a function of number of pixels for OSNR = 10 dB, $\kappa = 20.57$, 2-PAM pixel-matched system. Note that the solid line is (12), while points $\diamond$ are generated by numerically computing the mutual information.

signaling using a well known Monte Carlo technique [52]. Notice that the bound is tight and that a gain in the capacity of over two orders of magnitude is available by using multiple pixels over the case of using a single pixel for a given OSNR.

Although (12) demonstrates that increasing the number of pixels improves capacity, the same is true if the bandwidth, i.e., frame rate, of the channel is increased. Notice that if capacity is measured in bits per second, (12) demonstrates that increasing the bandwidth has the same impact as increasing the number of pixels. Thus, adding independent frames in time has the same impact on the capacity, in bits per second, as increasing the number of independent spatial channels. Thus, the key parameter in determining the capacity of the pixelated channel is the number of degrees of freedom arising from both temporal and spatial domains.

Qualitatively, the SNR in (11) follows the same relationship as results derived for CMOS active pixel sensors [40]. A common tradeoff for commercial imager designers is the one between improved spatial resolution with small pixel sizes and reduced per pixel SNR, which degrades image quality [44]. In the case of a pixelated wireless communications system, the criterion to optimize is the data throughput of the channel and not the perceived quality of the received image. As n increases, the SNR per pixel degrades and each subchannel is able to support modest data rates. However, the growth rate of the number of degrees of freedom grows faster realizing a net growth in channel capacity.

A similar result appears in radio channels with no fading, in which a spatial multiplexing gain is realized by employing a large number of spatial degrees of freedom for a fixed total power constraint [54], [55]. Thus, the pixelated wireless optical channel with its intrinsically high number of spatial degrees of freedom can realize significant gains in spectral efficiency over the single-element case. However, it should be noted that the gain over the single pixel case is only significant when high OSNRs are available.
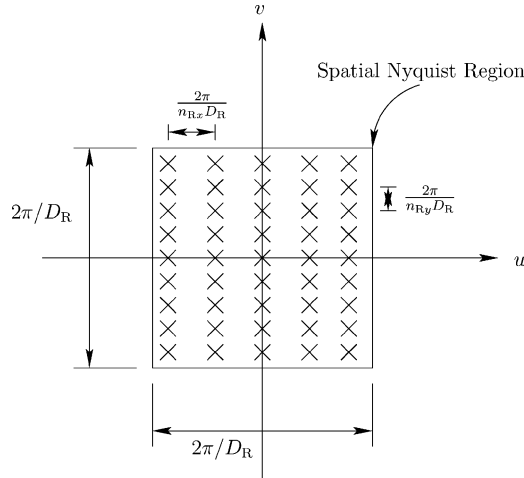
Fig. 6. Location of spatial frequency bins (represented by the $\times$) along with the spatial Nyquist region.

Such high-OSNR channels occur primarily in short-range wireless optical channels. Examples of such links include board-to-board and optical backplane applications as well as short-range interconnection applications. Long wavelength devices operating in the $1.3 \mu m$ wavelength range have larger permissible average optical power emissions over near infrared devices and can be used to improve OSNR. However, the cost of systems based on long wavelength devices is significantly higher since silicon photodetectors cannot be used.

B. Pixelated Channel Capacity: General Case

In general, pixelated wireless optical communication systems do not satisfy the strict alignment requirements imposed by the spatial Nyquist constraint imposed on $h_{\text{sys}}(x, y)$ in (9). In this section, we develop a capacity estimate for pixelated channels in which $h_{\text{sys}}(x, y)$ is a low-pass spatial response. We show that, as in the pixel-matched case, the key parameter in determining the channel capacity is the number of independent degrees of freedom provided for a given $h_{\text{sys}}, n_{\text{T}}$, and n_{R}. Contrary to previous work, interpixel crosstalk is treated explicitly in our estimate.

Without loss of generality, we consider the communications system in spatial frequency domain. At the transmitter, an image is formed by modulating data directly in spatial frequency domain, and then performing an inverse Fourier transform to yield the transmit image. To avoid aliasing, we assume that the transmitted image has no energy outside of the *spatial Nyquist region* [38], [56] of the receive sampler, as illustrated in Fig. 6. Consider forming transmit images by breaking spatial frequency domain into a discrete set of $n_{\text{T}x} \times n_{\text{T}y}$ *bins* as shown in the figure.

Since the transmit array has finite spatial dimensions $n_{\text{T}x} D'_{\text{T}} \times n_{\text{T}y} D'_{\text{T}}$, the independent spatial frequency bins are spaced at distances of $2\pi/n_{\text{T}x} D'_{\text{T}}$ and $2\pi/n_{\text{T}x} D'_{\text{T}}$, respectively in spatial frequency domain [56]. Similarly, the receive imager has finite spatial dimensions $n_{\text{R}x} D_{\text{R}} \times n_{\text{R}y} D_{\text{R}}$, and the independent spatial frequency bins in the Nyquist band are spaced at distances of $2\pi/n_{\text{R}x} D_{\text{R}}$ and $2\pi/n_{\text{R}x} D_{\text{R}}$. To ensure that the receiver is able to detect the spatial bins of the transmitter,

we assume that $n_{\text{T}x} D'_{\text{T}} = n_{\text{R}x} D_{\text{R}}$ and $n_{\text{T}y} D'_{\text{T}} = n_{\text{R}y} D_{\text{R}}$. In Section IV-B, we demonstrate formally that this is the condition required for spatial synchronization of the pixelated wireless optical channel.

Data is modulated in each spatial frequency bin by transmitting a complex amplitude, $A(u, v)$, in each bin and while ensuring Hermitian symmetry through the origin, i.e., $A(u, v) = A^*(-u, -v)$, where "$*$" denotes complex conjugate. In this model, the resulting transmitted images are periodic real-valued images of infinite extent. Assume that the receiver performs a Fourier transform on the input image and is able to detect the amplitude and phase of the spatial frequency component in each bin to give the measured values

$$R(u, v) = A(u, v)H_{\text{sys}}(u, v) + N(u, v) \qquad (13)$$

where $N(u, v)$ is the Fourier transform of the input noise process. Thus, the dispersive spatial channel can be treated as a series of parallel Gaussian channels in spatial frequency domain. In Section IV, we present a practical communication system for implementing a finite extent image transmitter, receiver and spatial synchronization algorithm satisfying the above communication system model.

Practical pixelated wireless optical channels are both peak-and average-amplitude limited. Since the capacity of these channels is not known in closed form, as was done in Section III-A, the capacity of the channel is estimated by approximating it as an AWGN channel with a modified electrical power constraint. Let the total electrical power constraint, E be a function of the average optical power constraint, P, as $E = cP^2$ for some constant $c > 0$. The dc spatial frequency bin of the power allocation is set to be the constant

$$A(0, 0) = n_{\text{T}} P$$

so that the average amplitude constraint is satisfied for every transmitted image. Although this assumption ensures that the average optical power constraint is met, it is pessimistic since in single-element channels it has been demonstrated that varying the optical bias per symbol can lead to significant gains in OSNR [19]. The constant c is chosen so that the clipping distortion of the channel is minimized. For a given bias optical power P, c is set to ensure that the probability of a negative amplitude is small. Any negative excursions by the signal are clipped and modeled as noise. Thus, an AWGN channel is used to give an estimate of the capacity of the pixelated wireless optical channel where the electrical constraint is set to ensure that the nonnegativity constraint is satisfied with high probability. Section III-B.2 presents a specific instance of this approximation for the prototype system.

In addition to shot noise and electronics noise, this channel is affected by spatially aliased noise due to the clipping and quantization distortion. The transmitter quantization noise is a result of the finite number of intensities, which can be emitted, while at the receiver, the number of bits in the analog-to-digital (A–D) converter of the image sensor introduce quantization noise. These noise components will, in general, be signal-dependent and correlated. In Section II-E, the variance of the receiver noise was shown to be nearly linearly dependent on

the input intensity level. In order to estimate the capacity, we make the pessimistic assumption that the noise variance over spatial frequency bins, $\sigma^2(u, v)$, is the maximum variance over all inputs and that the noise in each bin is independent.

From (13), the channel consists of a series of independent Gaussian spatial frequency channels. The capacity of the channel is well known to be [51, Sec. 10.4]

$$C = \sum_{u,v} \frac{W}{\kappa} \log \left(1 + \frac{\kappa E(u, v)}{2W\sigma^2(u, v)} \right) \quad \text{b/s} \qquad (14)$$

where W is the fractional power bandwidth, κ is the effective dimension, and the power allocation per spatial frequency bin is

$$E(u, v) =$$
$$\begin{cases} \nu - \sigma^2(u, v)/|H(u, v)|^2, & \text{if } \nu > \sigma^2(u, v)/|H(u, v)|^2, \\ 0, & \text{otherwise} \end{cases}$$
$$\qquad (15)$$

for some constant ν such that

$$\sum_{u,v} E(u, v) = cP^2. \qquad (16)$$

An optimal power allocation over the spatial frequency bins is determined by "pouring" the electrical power constraint cP^2 over the bins to occupy those spatial frequency bins with the lowest $\sigma^2(u, v)/|H(u, v)|^2$. This result mirrors previous results in radio channels in which the power constraint is distributed over the singular values of the channel matrix [54], [55]. Although this capacity estimate does not explicitly take into account the nonnegativity amplitude constraint, the capacity results are in fact pessimistic due to the restrictions placed on E to ensure a high probability of nonnegativity, the addition of clipping noise and the assumption of noise independence in each spatial frequency bin.

C. Example: Spatially Bandlimited Channel

It is difficult to draw general conclusions about the capacity of the pixelated wireless optical channel, since $H_{\text{sys}}(u, v)$ will vary depending on the link configuration. Consider the instructive but unrealizable example of a flat, strictly spatially bandlimited channel

$$H_{\text{sys}}(u, v) = \begin{cases} 1, & \text{if } u, v \in [-W_S, W_S] \\ 0, & \text{otherwise,} \end{cases}$$

with spatially white noise $\sigma^2(u, v) = \sigma^2$. This example is analogous to the pixel-matched channel considered in Section III-A except that data is modulated in spatial frequency domain. In this case, the power allocation (15) will equally distribute the power over all available spatial frequency bins. We assume that the model of (13) holds. Section IV demonstrates practical algorithms to achieve this condition. The number of spatial degrees of freedom present is limited by $n_{\text{T}}, n_{\text{R}}$ as well as the spatial bandwidth of the channel. If n is the total number of spatial degrees of freedom, the capacity can be estimated as

$$C = \frac{nW}{\kappa} \log \left(1 + \frac{c\kappa P^2}{2nW\sigma^2} \right) \quad \text{b/s} \qquad (17)$$

where the number of available spatial degrees of freedom are

$$n = \min \left\{ n_{\text{R}x}, n_{\text{T}x}, 2W_S \frac{n_{\text{R}x} D_{\text{R}}}{2\pi} \right\}$$
$$\times \min \left\{ n_{\text{R}y}, n_{\text{T}y}, 2W_S \frac{n_{\text{R}y} D_{\text{R}}}{2\pi} \right\}. \qquad (18)$$

The number of spatial degrees of freedom available depend on the number of available receiver or transmitter pixels. If the number of elements in (18) is limited by n_{T} or n_{R}, the pixelated wireless optical channel is termed *pixel-limited*, since increasing n_{T} or n_{R} increases the number of spatial degrees of freedom and hence the capacity of the channel. Similarly, if $2W_S < 2\pi/D_{\text{R}}$ or $2W_S < 2\pi/D'_{\text{T}}$, then the system is termed *spatially bandwidth-limited*, since for a fixed transmit array and imager size increasing the number of transmit or receive pixels does not add any new spatial degrees of freedom within the Nyquist band.

In short-range links, the OSNRs as well as the spatial bandwidths increase. For a given distance, the goal is to increase the number of degrees of freedom until the channel becomes spatially bandwidth limited. That is, the goal is to engineer the channel so that in (18), $n_{\text{T}} = n_{\text{R}}$ and

$$2W_S = \frac{2\pi}{D_{\text{R}}}.$$

Notice also that in (17), temporal degrees of freedom, represented in the bandwidth W, contribute equally as spatial degrees of freedom to the channel capacity expression.

Thus, short-range pixelated optical channels provide significant improvements in spectral efficiency, as is the case with pixel-matched systems, by fully exploiting spatial and temporal degrees of freedom provided by the channel. These gains in spectral efficiency are only significant in channels with sufficient OSNR, such as interconnection and short-range links.

D. Capacity Estimate for Prototype System

The capacity of the prototype pixelated optical system of Section II-D can be estimated using the measured values, described in Section II-E and the Appendix, as well as (14).

It is assumed that the transmit array has been calibrated to linearize the gamma distortion leaving only the dc shift due to ambient lighting. The average amplitude was set at $P = 117.5$ due to this amplitude shift measured in the gamma distortion measurements. Each pixel was assumed to be independent and Gaussian-distributed with mean P, as is conventional in modeling multicarrier systems. Using the total energy constraint in (16), it can be shown that the variance of each pixel under these assumptions is $cP^2/512^2$. The clipping probability can then be approximated as

$$P_{\text{clip}} \approx 2Q \left(\frac{P}{\sqrt{cP^2/512^2}} \right).$$

Setting P_{clip} to 10^{-8} gives a value of $c = 512^2 \times 0.03$.

Unlike the previous example, the noise was not modeled as being spatially white; rather, the noise variance in each bin was estimated by running 50 frames through the channel model with
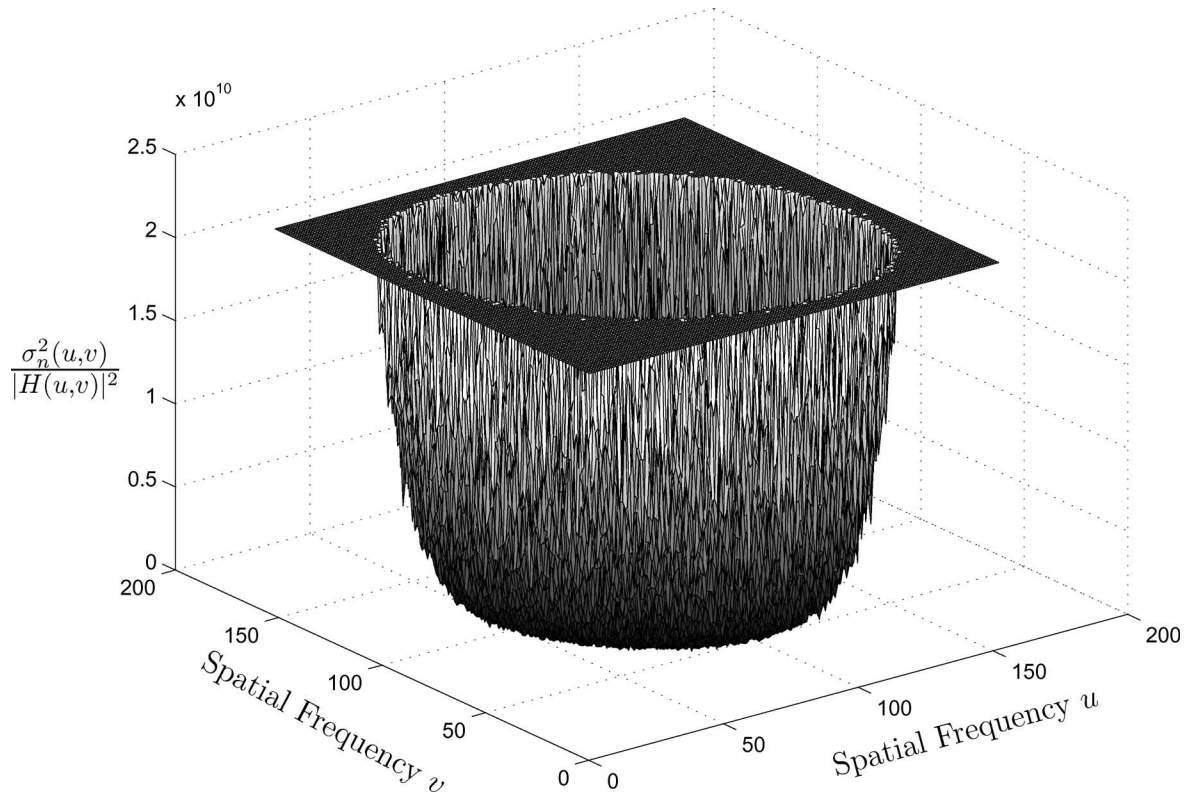
Fig. 7.   Water-pouring "bowl" for the prototype pixelated optical channel.

a power allocation, which spreads variance constraint amongst all channels evenly, and averaging the resulting noise variance per bin. The impact of quantization and clipping of the transmitter and receiver are quantified by including them in the noise estimate. Over many symbols, simulations verify that the resulting quantization distortion in the output image is small and well modeled as a broadband spatial frequency noise source.

Fig. 7 presents a plot of the water-pouring "bowl," $\sigma^2(u,v)/|H(u,v)|^2$, for the measured channel. The vertical axis in Fig. 7, is truncated to allow for plotting. The capacity of the channel, for the given frame rate, is estimated via (14) to be approximately 22.4 kb/frame. This capacity does not explicitly take into account the peak constraint of the channel, but rather models the channel as an electrical channel with added Gaussian clipping noise.

Pixel-matched signaling was also considered on this channel model by forming images with square blocks of pixels of size $L \times L$. Each pixel as modulated and detected independently. The maximum spectral efficiency of such a system over L is shown to be less than 290 b/s/Hz and is limited by crosstalk between the pixel channels [1].

IV. SDMT MODULATION

In the previous section, we discussed the capacity of spatially dispersive pixelated wireless optical systems by forming images in spatial frequency domain and taking the inverse Fourier transform. Using this motivation, we extend conventional multicarrier modulation for electrical channels to the spatially selective pixelated wireless optical channel.

In this section, we discuss practical algorithms to transmit data over pixelated wireless optical channels. Data is transmitted in spatial frequency domain by transmitting quadrature amplitude modulation (QAM) in each spatial frequency bin, as dictated by the water-pouring spectrum discussed in Section III-B.2. In order to approach the channel capacity, unoptimized error control techniques are applied to encode the symbols transmitted in each spatial frequency bin. We thus demonstrate that a majority of the capacity of the prototype system, estimated in Section III-B2, is realizable.

A. Definition

DMT modulation has been used in time dispersive channels and channels with narrow-band interferes such as digital subscriber lines [57], [58]. We extend conventional DMT to include spatial dimensions, i.e., we define SDMT modulation, in which data is transmitted by modulating in the spatial frequency domain.

Fig. 8 presents a block diagram of the SDMT system. The user data is coded and loaded in the spatial frequency domain dependent on the channel SNR in each frequency bin. It is assumed that there is a training period preceding data transmission in which test signals are transmitted to allow the receiver to determine the SNR in each spatial frequency bin and to feed it back to the transmitter. The transmitter can then compute a power allocation via (15) and load the spatial frequency bins appropriately. Section III-B2 presents a power allocation for an experimental channel.
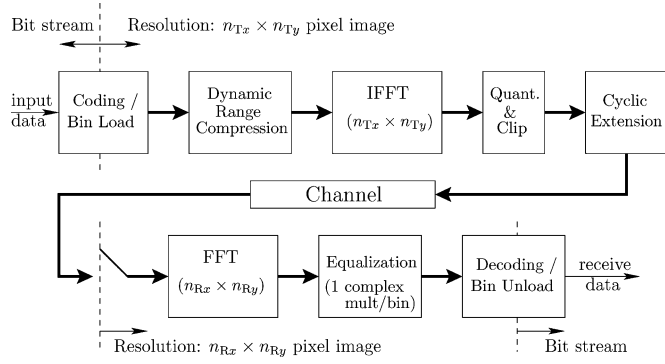
Fig. 8. Block diagram of the SDMT system.

After loading the bins, the resulting signal often exhibits a large peak-to-average ratio. This is a problem well known in conventional DMT systems [58]. The high peak-to-average ratio problem is especially acute in this channel due to the potentially large number of spatial degrees of freedom. Many techniques exist to reduce the dynamic range of the output signal through coding or exploiting unused spatial frequency bins [59]–[61].

The transmitted image is formed by taking the inverse fast Fourier transform (IFFT) of the $n_{\mathrm{T}x} \times n_{\mathrm{T}y}$ pixel image. As shown in Fig. 1, a *cyclic extension* is appended around the edges of the transmitted frame in order to ease the task of equalization at the receiver and is analogous to the cyclic prefix added in conventional DMT systems [57], [62]. Here, we assume that $h_{\mathrm{sys}}(x, y)$ in (8) can be well modeled by a finite impulse response model. A cyclic extension of size at least half of the channel memory, is appended around the data portion of the image to ensure that the finite extent of the image does not violate the periodicity assumption of the fast Fourier transform (FFT). Since there is no notion of causality in the image, appending an extension of half the channel memory to each side of the image is analogous to time-based systems in which the cyclic prefix length equals the channel memory. As a result, the linear convolution of the channel response with the image is equivalent to a circular convolution and so equalization at the receiver is a matter of a single complex multiplication per bin. This simplified channel is shown formally in (22) in Section IV-B, once spatial synchronization has been achieved.

For the prototype, the appended cyclic extension was 8 pixels wide. The use of a cyclic prefix uses pixels of the transmitter to transmit redundant information and constitutes an overhead on the communications system. In this case, the cyclic prefix imposes an overhead of 6.3% increase in the number of required transmit pixels for a given image size.

The receiver samples the incoming intensity signal in space. Since no spatial filtering is available, aliasing is an impairment at the front end of the receiver. Although the transmitted signal has no energy beyond the spatial Nyquist band [38], [56] of the receive array, the clipping and quantization noise generated in the transmitter are aliased. The received image is placed in frequency domain using $n_{\mathrm{R}x} \times n_{\mathrm{R}y}$ point FFT. The resulting spatial frequency bins are equalized, decoded, and unloaded. Thus, SDMT modulation provides a basis for spatially ban-

dlimited signals and tailors the transmitted image to minimize the impact of the spatial distortion of the channel.

B. Spatial Synchronization For SDMT

The receiver samples the incoming image at a rate specified by the spacing of the pixels in the receive array. Since the transmitted image is designed so that it lies within the spatial Nyquist region of the receiver, $r[k, l; iT]$ contains all transmitted data. Unlike time-based systems, it is not possible to spatially synchronize the receiver to the transmit image since the spacing and location of the receiver pixels is fixed. However, it is not necessary to match the frequency or phase of transmitted image at the receiver, as a free-running sampler operating above the spatial Nyquist rate is enough to ensure no information is lost [63].

In the present system, consider a single frame of a transmitted $n_{\mathrm{T}x} \times n_{\mathrm{T}y}$ pixel image with complex frequency domain coefficients $A[u, v]$ and let $H_{\mathrm{sys}}[u, v]$ be the sampled Fourier spectrum of $h_{\mathrm{sys}}(x, y)$. If the cyclic extension is added to the transmit frame, the resulting received image can be modeled as the periodic image

$$r(x, y) = \frac{1}{n_{\mathrm{T}}} \sum_{u,v} H_{\mathrm{sys}}[u, v] A[u, v]$$

$$\times \exp\left(2\pi j \frac{1}{D'_{\mathrm{T}}}\left(\frac{ux}{n_{\mathrm{T}x}} + \frac{vy}{n_{\mathrm{T}y}}\right)\right). \quad (19)$$

The CCD spatial sampler is a rectangular "bed-of-nails" yielding the spatially sampled response, $r[k, l] = r(x, y)|_{x=D_{\mathrm{R}}k, y=D_{\mathrm{R}}l}$. The received frequency domain signal, $R[w, z; iT]$, is defined as the $n_{\mathrm{R}x} \times n_{\mathrm{R}y}$ point FFT of $r[k, l; iT]$

$$R[w, z] = \sum_{k,l} r[k, l] \exp\left(-2\pi j \left(\frac{kw}{n_{\mathrm{R}x}} + \frac{lz}{n_{\mathrm{R}y}}\right)\right).$$

Substituting (19) and expanding the sums over k, l gives

$$R[w, z] = \frac{1}{n_{\mathrm{T}}} \sum_{u,v} H_{\mathrm{sys}}[u, v] A[u, v]$$

$$\sum_{k=0}^{n_{\mathrm{R}x}-1} W_{n_{\mathrm{R}x}}^{\frac{n_{\mathrm{R}x} D_{\mathrm{R}}}{n_{\mathrm{T}x} D'_{\mathrm{T}}} uk} W_{n_{\mathrm{R}x}}^{-kw} \sum_{l=0}^{n_{\mathrm{R}y}-1} W_{n_{\mathrm{R}y}}^{\frac{n_{\mathrm{R}y} D_{\mathrm{R}}}{n_{\mathrm{T}y} D'_{\mathrm{T}}} vl} W_{n_{\mathrm{R}y}}^{-lz} \quad (20)$$

where $W_M = \exp(j2\pi/M)$. Notice that the last two terms in (20) can be viewed as $n_{\mathrm{R}x}$- and $n_{\mathrm{R}y}$-point discrete Fourier transforms, respectively. If

$$n_{\mathrm{R}x} D_{\mathrm{R}} = n_{\mathrm{T}x} D'_{\mathrm{T}} \quad \text{and} \quad n_{\mathrm{R}y} D_{\mathrm{R}} = n_{\mathrm{T}y} D'_{\mathrm{T}} \quad (21)$$

then

$$R[w, z] = \frac{n_{\mathrm{R}}}{n_{\mathrm{T}}} \sum_{u,v=0}^{N-1} H_{\mathrm{sys}}[u, v] A[u, v] \delta[(u - w) \bmod n_{\mathrm{R}x}]$$

$$\times \delta[(v - z) \bmod n_{\mathrm{R}y}].$$

If the transmit spectrum is bandlimited to the Nyquist rate of the receive spatial sampler, i.e., $A[u, v] = 0$ for $u \notin$

$\{0, 1, \ldots, n_{Rx} - 1\}$ and $v \notin \{0, 1, \ldots, n_{Ry} - 1\}$, then

$$R[w, z] = \frac{n_R}{n_T} H_{sys}[w, z] A[w, z]. \qquad (22)$$

Notice that equalization in each spatial frequency bin consists of a single complex multiplication. If the conditions (21) are not satisfied, the frequency resolution of transmitter and receiver are not identical and ICI is unavoidable. Thus, the synchronization problem reduces to one of ensuring that the dimensions of the projected transmit image are an integer number of receive imager sampling instants. Note that in the case of transmitting a square array, $n_{Tx} = n_{Ty}$, the conditions in (21) are equivalent. If a multifocal length lens is available at the camera, then the scale of the transmit image in the receive plane can be appropriately adjusted. If, as assumed, the input is sampled at a rate higher than its Nyquist frequency, it is possible to interpolate such that the condition is satisfied. A consequence of this is that the cyclic extension must be increased by half of the size of the interpolation filter memory.

C. Coding Implementation

The capacity of the SDMT pixelated channel estimates the maximum achievable rate per channel use (i.e., per frame); however, it does not suggest any realizable method to achieve the rates. In this section, we apply conventional, unoptimized codes to the pixelated channel and show that a significant portion of the channel capacity can be realized in practice.

Multilevel codes are a coded modulation scheme that use binary codes to improve the reliability of multilevel QAM constellations [64]. For constellations of size 2^M, M address bits, $B = (b_0, b_1, \ldots, b_{M-1})$, are required to label each constellation point. A multilevel coding scheme assigns a binary code, C_i, to each b_i depending on the "quality" of the given bit channel. Formally, if Y is the received variable, then the mutual information can be written as

$$I(Y; B) = I(Y; b_0, b_1, \ldots, b_M)$$
$$= I(Y; b_0) + I(Y; b_1|b_0) + \cdots$$
$$+ I(Y; b_{M-1}|b_0, b_1, \ldots, b_{M-2}).$$

Thus, data transmission on this channel can be modeled as communication on M parallel bit channels, b_i, assuming $b_0, \ldots, b_{i-1}$ are known [65]. If each code C_i is capacity achieving, then the total channel capacity is achieved using multilevel coding and multistage decoding [65].

For conventional DMT channels, it has been found that the use of multilevel codes can approach the channel capacity over a wide class of channels [66], [67], [68]. Following [68], we design a multilevel coder and multistage decoder for the SDMT system, presented in Figs. 9 and 10. The least significant bits b_0 and b_1 in each bin are gray labeled and treated as a single symbol. The average capacity of $b_0 b_1$ over all the frequency bins was computed as 0.56 b/symbol. Bits $b_0 b_1$ in each spatial frequency bin are coded with a near capacity achieving, irregular rate-1/2 low density parity check code with block length 10^5 [68]. The higher level bits are labeled using Ungerboeck's set partitioning labeling. A target bit error rate (BER) of 10^{-7} was set and the
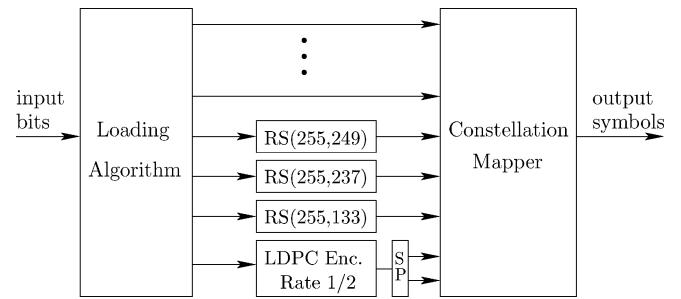

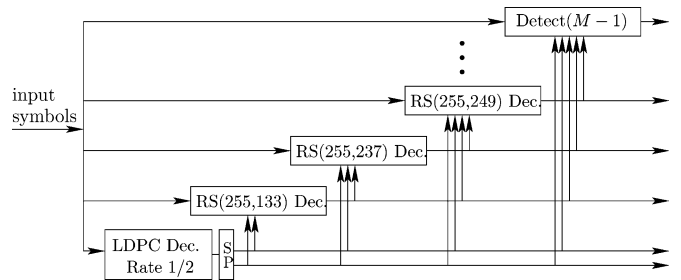Fig. 9. Multilevel coder block diagram for the SDMT channel.

Fig. 10. Multistage decoder for the SDMT channel.

TABLE I
CODE DESIGN FOR HIGHER LEVEL BIT LABELS

Bit	Pe(b_i|$b_0 \ldots b_{i-1}$)	Capacity of BSC	RS Code	Code Rate
b_2	0.01598	0.8818	(255,133)	0.5216
b_3	3.5258×10^{-4}	0.9954	(255,237)	0.9294
b_4	1.0371×10^{-6}	0.9999	(255,249)	0.9765
b_5	1.6014×10^{-11}	-	uncoded	-

upper bit channels were modeled as binary symmetric channels (BSCs). Hard decision Reed—Solomon codes of block length 255 were applied to correct enough errors to ensure that the target error rate was met and are presented in Table I along with the average conditional probability of error and the capacity of the associated BSCs. For b_5 and higher label bits, uncoded transmission satisfies the BER target.

After applying multilevel codes, the resulting rate is 17.1 kb/frame or 76% of the estimated channel capacity. The resulting spectral efficiency of the system using rectangular PAM modulation for each pixel and a 99% fractional power definition of bandwidth is 1.7 kb/s/Hz.

V. CONCLUSION AND FUTURE DIRECTIONS

We have shown in this paper that transmitting and detecting a series of images composed of millions of pixels is a promising technique to provide extremely high-rate short-range wireless optical links. The pixelated wireless optical channel realizes these gains in spectral efficiency by exploiting the spatial degrees of freedom inherent to the large number of emitter and detector elements. Unlike previous multielement optical links, spatial multiplexing gains are achieved without the need for the precise spatial alignment. Spatio-temporal coding over time and spatial degrees of freedom is key to realizing these increased

spectral efficiencies and replaces the inefficient spatial repetition code of conventional multielement wireless optical links.

The pixelated wireless optical channel is ideally suited to applications that require high-speed short range communication links, in which a line-of-sight is available. For interconnect and data exchange applications, the pixelated channel is attractive due to the availability of moderately priced components, unregulated bandwidth, compact size, and freedom from near-field effects in current radio links. The pixelated wireless optical link is also promising for short-range indoor wireless optical communications due to its extremely high spectral efficiencies. However, due to the requirement for line-of-sight and limited emitted optical power, it is anticipated that these links are complements, rather than replacements, for indoor mobile radio links.

Another suitable area of application of the pixelated optical channel is in situations that require strict signal containment. Examples of such applications include communications within a room or in some enclosure, or perhaps between two communicating parties concerned about radiating to an unauthorized third party. Such signal containment is easily achieved with optical signals, but is in general far more difficult to achieve with RF signals. Such signal containment would also allow for aggressive spatial reuse of optical frequencies.

To extend the application of the pixelated channel, the operation must be generalized beyond the on-axis case. Compensation of rotational, scale and projective distortions and their impact on capacity is still an open question. The complexity of implementing the spatio-temporal coding needs to be considered in practical systems. Lower complexity precoding and 2-D partial response schemes may also be appropriate on this channel. The planar transmitters and receivers considered in this work can be generalized in future pixelated optical links. The use of flexible OLED panels promise the possibility of inexpensive hemispherical arrays to reduce the alignment sensitivity of point-to-point links. Additionally, the theory and techniques presented here for pixelated wireless communications can be employed in a range of wavelengths including infrared and visible domain.

The goal of this work has been to demonstrate the immense gains available through the use of spatio-temporal coding in short-range MIMO wireless optical channels. It is anticipated that continued work on this channel will lead not only to a rich source of interesting research topics but also to a host of potential applications.

APPENDIX

PROTOTYPE MEASUREMENT TECHNIQUES

This appendix provides additional details on the measurement technique used on the prototype channel presented in Section II-D.

In order to measure the spatial response of the channel, represented by $h_{\mathrm{sys}}(x,y)$ in (8), individual pixels were illuminated at the transmitter at a variety of locations. For each location, the measured image was averaged over 10 000 frames to form an estimate of the point-spread function. The zero-input response of the channel was also averaged over 10 000 frames to remove
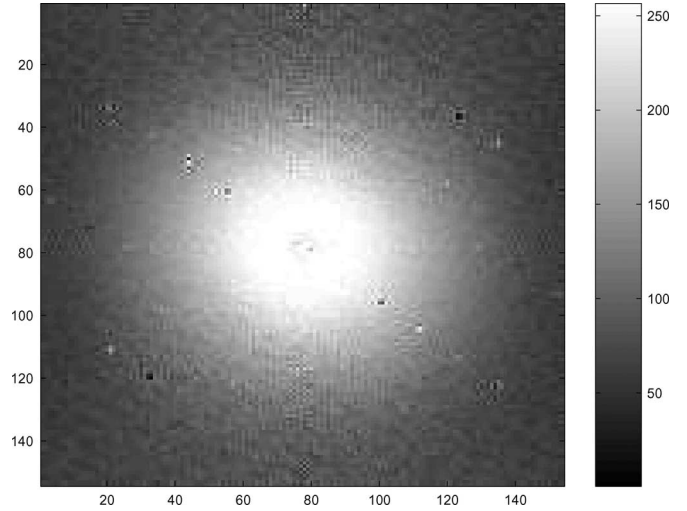

Fig. 11.   Magnitude of OTF for center pixel of prototype.

offsets caused by systematic intensity variations over the LCD panel. Fig. 11 presents the magnitude of the OTF for the central transmitted pixel. Notice that the response is low pass in spatial frequency domain. Using these end-to-end measurements, it is not possible to determine the factors in (5) but only to find the system point-spread function. Similar measurements were repeated at various points over the array. After correcting for the phase shift of each measured point, the peak discrepancy between the central point and the measured responses is less than 9% in terms of the energy. Although it is evident that there is some spatial dependence on the point-spread function, the assumption of spatial invariance holds approximately since the variations are small. In order to get a closed-form expression for $h_{\mathrm{sys}}(x,y)$, a Gaussian pulse was fitted to the measured OTF as is conventionally done in the analysis of some commercial video equipment [69]. The Gaussian fit for the OTF of the central pixel is

$$H_{\mathrm{sys}}(u,v) = K \exp\left(-\frac{u^2}{2\sigma_u^2} - \frac{v^2}{2\sigma_v^2}\right)$$

where u,v are in discrete spatial frequency domain, $K = 200.44$, $\sigma_u^2 = 1681.78$, and $\sigma_v^2 = 1751.76$. Taking the inverse Fourier transform gives an estimate for $h_{\mathrm{sys}}(x,y)$ as

$$h_{\mathrm{sys}}(x,y) = KD_R^2 \frac{\sigma_u' \sigma_v'}{2\pi} \exp\left(-\frac{x^2}{2/\sigma_u'^2} - \frac{y^2}{2/\sigma_v'^2}\right)$$

where

$$\sigma_u' = \sigma_u \frac{2\pi}{154 D_{\mathrm{R}}} \quad \text{and} \quad \sigma_v' = \sigma_v \frac{2\pi}{154 D_{\mathrm{R}}}$$

are normalized standard deviations continuous in spatial domain.

Cathode ray tubes and LCD panels have a nonlinear *gamma distortion* between the input level and the optical intensity output [40]. In order to measure the gamma distortion for the display used in the link, the transmit image was set to be a constant gray value between 0 and 256. The receive images are averaged over 1000 frames to produce an estimate of the received intensity
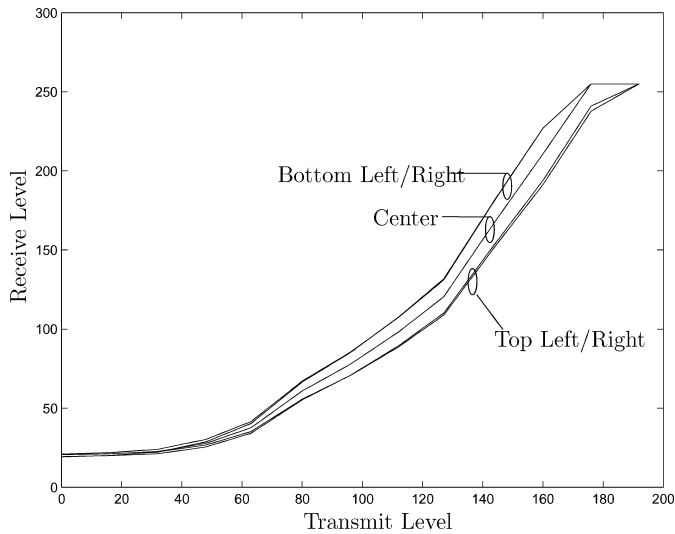
Fig. 12.   Measured gamma distortion of transmitter as a function of intensity and position along with least-squares linear fit for prototype.
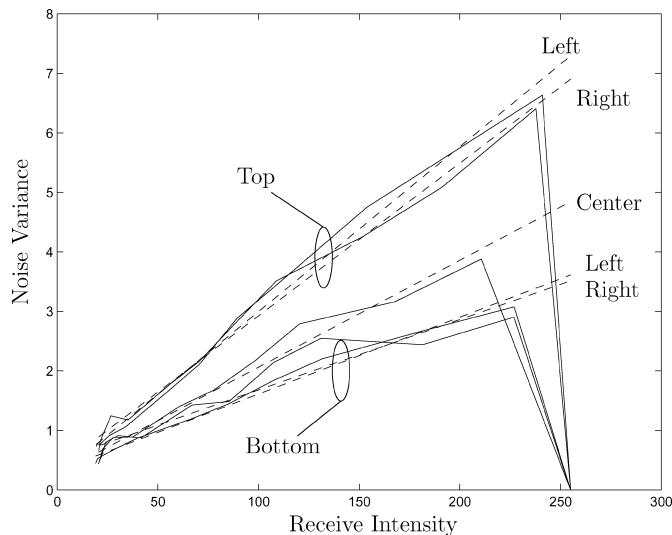

Fig. 13.   Variance of receiver noise as a function of intensity and position along with least-squares linear fit for prototype.

value in the absence of noise. Fig. 12 presents the measured gamma distortion at five locations on the transmit array. The nonlinear distortion of the channel is spatially dependent, and the average response over a variety of positions is used as the prototypical gamma distortion of the channel. A least-squares fit of the average gamma response was performed to the classical response [40] to yield

$$J(x,y) = 1.1 \times 10^{-3} I(x,y)^{2.4} + 20.2$$

where $I(x,y)$ is the input image and $J(x,y)$ is the corresponding output.

The noise at each receive pixel is due to background light as well as due to the transmitted signal. As discussed in Section II, the distribution of this noise is typically taken as being Gaussian with variance linearly related to the receive intensity. The variance of the noise was averaged over five locations

TABLE II
MINIMUM MEAN SQUARE FIT OF VARIANCE TO THE MODEL $\sigma_i^2(x) = \alpha x + \beta$ ALONG WITH R^2 STATISTIC OF FIT

	α	β	R^2
Top Left	0.0277	0.2250	0.9948
Top Right	0.0256	0.3616	0.9921
Center	0.0180	0.2657	0.9801
Bottom Left	0.0129	0.3208	0.9879
Bottom Right	0.0118	0.4981	0.9134

and 1000 frames. Fig. 13 plots the change in the variance as a function of the transmitted level under normal background illumination levels. Note that at high received values, the quantizer saturates the receive value and the variance goes to zero. Table II presents the linear fit to the measured responses and the R^2 statistic of fit [70], where R^2 near one indicates a good fit. The noise is modeled as being independent in both time and space. This is a worst case scenario since any correlation in the noise could be exploited in detection. For the channel model, the average value for α and β over the five locations is used. The resulting variance as a function of position is

$$\sigma^2(x,y) = 1.9 \times 10^{-2} \mathsf{i}_R(x,y) + 0.33 \quad [\mathsf{A}^2]$$

satisfying the noise model given in (7).

REFERENCES

[1] S. Hranilovic, "Spectrally efficient signalling for wireless optical intensity channels" Ph.D. dissertation, Dept. Elect. Comput. Eng., Univ. Toronto, Toronto, ON, Canada, 2003.

[2] ——, *Wireless Optical Communication Systems*.   New York: Springer, 2004.

[3] ——, "On the design of bandwidth efficient signalling for indoor wireless optical channels," *Int. J. Commun. Syst.*, vol. 18, no. 3, pp. 205–228, Apr. 2005.

[4] H. F. Bare, F. Haas, D. A. Honey, D. Mikolas, H. G. Craighead, G. Pugh, and R. Soave, "A simple surface-emitting LED array useful for developing free-space optical interconnects," *IEEE Photon. Technol. Lett.*, vol. 5, no. 2, pp. 172–174, Feb. 1993.

[5] M. A. Neifeld and R. K. Kostuk, "Error correction for free-space optical interconnects: Space-time resource optimization," *Opt. Lett.*, vol. 37, no. 2, pp. 296–307, Jan. 1998.

[6] D. V. Plant and A. G. Kirk, "Optical interconnects at the chip and board level: Challenges and solutions," *Proc. IEEE*, vol. 88, no. 6, pp. 806–818, Jun. 2000.

[7] T. H. Szymanski, "Bandwidth optimization of optical data link by use of error-control codes," *Opt. Lett.*, vol. 39, no. 11, pp. 1761–1775, Apr. 2000.

[8] D. V. Plant, M. B. Venditti, E. Laprise, J. Faucher, K. Razavi, M. Châteauneuf, A. G. Kirk, and J. S. Ahearn, "256-channel bidirectional optical interconnect using VCSELs and photodiodes on cmos," *J. Lightw. Technol.*, vol. 19, no. 8, pp. 1093–1103, Aug. 2001.

[9] M. Châteauneuf, A. G. Kirk, D. V. Plant, T. Yamamoto, and J. D. Ahearn, "512-channel vertical-cavity surface-emitting laser based free-space optical link," *J. Lightw. Technol.*, vol. 41, no. 26, pp. 5552–5561, Sep. 2002.

[10] J. Faucher, M. B. Venditti, and D. V. Plant, "Application of parallel forward-error correction in two-dimensional optical-data links," *J. Lightw. Technol.*, vol. 21, no. 2, pp. 466–475, Feb. 2003.

[11] G. W. Burr, J. Ashley, H. Coufal, R. K. Grygier, J. A. Hoffnagle, C. Michael Jefferson, and B. Marcus, "Modulation coding for pixel-matched holographic data storage," *Opt. Lett.*, vol. 22, no. 9, pp. 639–641, May 1997.

[12] F. R. Gfeller and U. Bapst, "Wireless in-house communication via diffuse infrared radiation," *Proc. IEEE*, vol. 67, no. 11, pp. 1474–1486, Nov. 1979.

[13] J. M. Kahn and J. R. Barry, "Wireless infrared communications," *Proc. IEEE*, vol. 85, no. 2, pp. 263–298, Feb. 1997.

[14] D. R. Wisely, "A 1 Gbit/s optical wireless tracked architecture for ATM delivery," in *IEE Colloq. Optical Free-Space Commun. Links*, 1996, pp. 1411–1417.

[15] J. R. Barry, *Wireless Infrared Communications*. Boston, MA: Kluwer, 1994.

[16] D. Shiu and J. M. Kahn, "Shaping and nonequiprobable signalling for intensity-modulated signals," *IEEE Trans. Inf. Theory*, vol. 45, no. 7, pp. 2661–2668, Nov. 1999.

[17] H. Sugiyama and K. Nosu, "MPPM: A method for improving the band-utilization efficiency in optical PPM," *J. Lightw. Technol.*, vol. 7, no. 3, pp. 465–472, Mar. 1989.

[18] H. Park and J. R. Barry, "Modulation analysis for wireless infrared communications," in *Proc. IEEE Int. Conf. Commun.*, 1995, pp. 1182–1186.

[19] S. Hranilovic and D. A. Johns, "A multilevel modulation scheme for high-speed wireless infrared communications," in *Proc. IEEE ISCAS*, 1999, vol. VI, pp. 338–341.

[20] A. Garcia-Zambrana and A. Puerta-Notario, "Improving PPM schemes in wireless infrared links at high bit rates," *IEEE Commun. Lett.*, vol. 5, no. 3, pp. 95–97, Mar. 2001.

[21] J. B. Carruthers and J. M. Kahn, "Multiple-subcarrier modulation for nondirected wireless infrared communication," *IEEE J. Sel. Areas Commun.*, vol. 14, no. 3, pp. 538–546, Apr. 1996.

[22] ——, "Angle diversity for nondirected wireless infrared communication," *IEEE Trans. Commun.*, vol. 48, no. 6, pp. 960–969, Jun. 2000.

[23] S. Jivkova and M. Kavehrad, "Receiver designs and channel characterization for multi-spot high-bit-rate wireless infrared communications," *IEEE Trans. Commun.*, vol. 49, no. 12, pp. 2145–2153, Dec. 2001.

[24] G. Yun and M. Kavehrad, "Spot-diffusing and fly-eye receivers for indoor infrared wireless coummunications," in *Proc. IEEE Int. Conf. Sel. Topics Wireless Commun.*, 1992, pp. 262–265.

[25] P. Djahani and J. M. Kahn, "Analysis of infrared wireless links employing multibeam transmitters and imaging diversity receivers," *IEEE Trans. Commun.*, vol. 48, no. 12, pp. 2077–2088, Dec. 2000.

[26] J. M. Kahn, R. You, P. Djahani, A. G. Weisbin, B. K. Teik, and A. Tang, "Imaging diversity receivers for high-speed infrared wireless communication," *IEEE Commun. Mag.*, vol. 36, no. 12, pp. 88–94, Dec. 1998.

[27] K. Akhavan, M. Kavehrad, and S. Jivkova, "High-speed power-efficient indoor wireless infrared communication using code combining—Part I," *IEEE Trans. Commun.*, vol. 50, no. 7, pp. 1098–1109, Jul. 2002.

[28] ——, "High-speed power-efficient indoor wireless infrared communication using code combining—Part II," *IEEE Trans. Commun.*, vol. 50, no. 9, pp. 1495–1502, Sep. 2002.

[29] S. M. Haas, J. H. Shapiro, and V. Tarokh, "Space-time codes for wireless optical communications," *EURASIP J. Appl. Sig. Proc.*, vol. 2002, no. 3, pp. 211–220, Mar. 2002.

[30] J. M. Kahn, W. J. Krause, and J. B. Carruthers, "Experimental characterization of non-directed indoor infrared channels," *IEEE Trans. Commun.*, vol. 43, no. 2–4, pp. 1613–1623, Feb.–Apr. 1995.

[31] B. G. Boone, *Signal Processing Using Optics: Fundamentals, Devices, Architectures, and Applications*. New York: Oxford Univ. Press, 1998.

[32] R. Klette, K. Schlüns, and A. Koschan, *Computer Vision: Three-Dimensional Data from Images*. Singapore: Springer-Verlag, 1998.

[33] Silicon Optix Inc. [Online]. Available: http://www.siliconoptix.com

[34] D. P. Petersen and D. Middleton, "Sampling and reconstruction of wavenumber-limited functions in n-dimensional Euclidean spaces," *Inf. Control.*, vol. 5, pp. 279–323, 1962.

[35] R. M. Mersereau, "The processing of hexagonally sampled two-dimensional signals," *Proc. IEEE*, vol. 67, no. 6, pp. 930–949, Jun. 1979.

[36] V. Vilnrotter, C. W. Lau, M. Srinivasan, K. Andrews, and R. Mukai, "Optical array receiver for communication through atmospheric turbulence," *J. Lightw. Technol.*, vol. 23, no. 4, pp. 1664–1675, Apr. 2005.

[37] A. M. Bruckstein, L. O'Gorman, and A. Orlitsky, "Design of shapes for precise image registration," *IEEE Trans. Inf. Theory*, vol. 44, no. 7, pp. 3156–3162, Nov. 1998.

[38] J. W. Goodman, *Introduction to Fourier Optics*, 3rd ed. Englewood, CO: Roberts, 2005.

[39] K. H. Mueller and M. Müller, "Timing recovery in digital synchronous data receivers," *IEEE Trans. Commun.*, vol. COM-24, no. 5, pp. 516–531, May 1976.

[40] G. C. Holst, *CCD Arrays, Cameras, and Displays*, 2nd ed. Bellingham, WA: SPIE, 1998.

[41] J. R. Janesick, *Scientific Charge-Coupled Devices*. Bellingham, WA: SPIE, 2001.

[42] E. G. Stevens, "A unified model of carrier diffusion and sampling aperture effects on MTF in solid-state image sensors," *IEEE Trans. Electron Devices*, vol. 39, no. 11, pp. 2621–2623, Nov. 1992.

[43] H. Tian and A. El Gamal, "Analysis of temporal noise in CMOS photodiode active pixel sensor," *IEEE J. Solid-State Circuits*, vol. 36, no. 1, pp. 92–101, Jan. 2001.

[44] T. Chen, P. Catrysse, A. El Gamal, and B. Wandell, "How small should pixel size be?," *Proc. SPIE*, vol. 3965, pp. 451–459, 2000.

[45] S. K. Mendis, S. E. Kemeny, R. C. Gee, B. Pain, C. O. Staller, Q. Kim, and E. R. Fossum, "CMOS active pixel image sensors for highly integrated imaging systems," *IEEE J. Solid-State Circuits*, vol. 32, no. 2, pp. 187–197, Feb. 1997.

[46] S. Hranilovic and F. R. Kschischang, "Short-range wireless optical communication using pixelated transmitters and imaging receivers," in *Proc. IEEE Int. Conf. Commun.*, 2004, pp. 891–895.

[47] C. E. Shannon, "A mathematical theory of communication," *Bell Syst. Tech. J.*, vol. 27, pp. 379–423, Jul.–Oct. 1948.

[48] H. Nyquist, "Certain topics in telegraph transmission theory," *Trans. AIEE*, vol. 47, pp. 617–644, Apr. 1928.

[49] S. Hranilovic and F. R. Kschischang, "Optical intensity-modulated direct detection channels: Signal space and lattice codes," *IEEE Trans. Inf. Theory*, vol. 49, no. 6, pp. 1385–1399, Jun. 2003.

[50] ——, "Capacity bounds for power- and band-limited optical intensity channels corrupted by Gaussian noise," *IEEE Trans. Inf. Theory*, vol. 50, no. 5, pp. 784–795, May 2004.

[51] T. M. Cover and J. A. Thomas, *Elements of Information Theory*. New York: Wiley, 1991.

[52] G. Ungerboeck, "Channel coding with multilevel/phase signals," *IEEE Trans. Inf. Theory*, vol. IT-28, no. 1, pp. 55–67, Jan. 1982.

[53] H. J. Landau and H. O. Pollak, "Prolate spheroidal wave functions, Fourier analysis and uncertainty—III: The dimension of the space of essentially time- and band-limited signals," *Bell Syst. Tech. J.*, vol. 41, pp. 1295–1336, Jul. 1962.

[54] G. J. Foschini and M. J. Gans, "On limits of wireless communications in a fading environment when using multiple antennas," *Wireless Pers. Commun.*, vol. 6, no. 3, pp. 311–335, Mar. 1998.

[55] I. E. Telatar, "Capacity of multi-antenna Gaussian channels," *Eur. Trans. Telecommun.*, vol. 10, no. 6, pp. 585–595, Nov./Dec. 1999.

[56] R. C. Gonzalez and R. E. Woods, *Digital Image Processing*. Reading, MA: Addison-Wesley, 1992.

[57] J. S. Chow, J. C. Tu, and J. M. Cioffi, "A discrete multitone transceiver system for HDSL applications," *IEEE J. Sel. Areas Commun.*, vol. 9, no. 6, pp. 895–908, Aug. 1991.

[58] J. A. C. Bingham, "Multicarrier modulation for data transmission: An idea whose time has come," *IEEE Commun. Mag.*, pp. 5–14, May 1990.

[59] A. Gatherer and M. Polley, "Controlling clipping probability in DMT transmission," in *Proc. 31st Asilomar Conf. Signals, Systems & Computers*, 1997, vol. 1, pp. 578–584.

[60] K. G. Paterson and V. Tarokh, "On the existence and construction of good codes with low peak-to-average power ratios," *IEEE Trans. Inf. Theory*, vol. 46, no. 6, pp. 1974–1987, Sep. 2000.

[61] R. You and J. M. Kahn, "Average power reduction techniques for multiple-subcarrier intensity-modulated optical signals," *IEEE Trans. Commun.*, vol. 49, no. 12, pp. 2164–2171, Dec. 2001.

[62] A. Peled and A. Ruiz, "Frequency domain data transmission using reduced computational complexity algorithms," in *Proc. IEEE Int. Conf. Acoust., Speech, Signal Process.*, 1980, vol. 5, pp. 964–967.

[63] H. Meyr and A. Polydoros, "On sampling rate, analog prefiltering, and sufficient statistics for digital receivers," *IEEE Trans. Commun.*, vol. 42, no. 12, pp. 3208–3214, Dec. 1994.

[64] H. Imai and S. Hirakawa, "A new multilevel coding method using error-correcting codes," *IEEE Trans. Inf. Theory*, vol. 23, no. 3, pp. 371–377, May 1977.

[65] U. Wachsmann, R. F. H. Fischer, and J. B. Huber, "Multilevel codes: Theoretical concepts and practical design rules," *IEEE Trans. Inf. Theory*, vol. 45, no. 5, pp. 1361–1391, Jul. 1999.

[66] L. Zhang and A. Yongacoglu, "Turbo coding in ADSL DMT systems," in *Proc. IEEE Int. Conf. Commun.*, 2001, vol. 1, pp. 151–155.

[67] E. Eleftheriou and S. Ölçer, "Low-density parity-check codes for digital subscriber lines," in *Proc. IEEE Int. Conf. Commun.*, 2002, pp. 1752–1757.

[68] M. Ardakani, T. Esmailian, and F. R. Kschischang, "Near-capacity coding in multi-carrier modulation systems," *IEEE Trans. Commun.*, vol. 52, no. 11, pp. 1880–1889, Nov. 2004.

[69] W. F. Schreiber, *Fundamentals of Electronic Imaging Systems: Some Aspects of Image Processing*, 3rd ed. Berlin, Germany: Springer-Verlag, 1993.

[70] N. R. Draper and H. Smith, *Applied Regression Analysis*, 2nd ed. New York: Wiley, 1981.

Steve Hranilovic (S'94–M'03) received the B.A.Sc. (Honors) degree from the University of Waterloo, Waterloo, ON, Canada in 1997, and the M.A.Sc. and Ph.D. degrees from the University of Toronto, Toronto, ON, Canada, in 1999 and 2003, respectively, all in electrical engineering.

From 1992 to 1997, while studying for the B.A.Sc. degree, he worked in the areas of semiconductor device characterization and microelectronics for Nortel Networks and the VLSI Research Group, University of Waterloo. Currently, he is an Assistant Professor in the Department of Electrical and Computer Engineering, McMaster University, Hamilton, ON, Canada. He is the author of the book *Wireless Optical Communications Systems* (Springer-Verlag, 2004). His research interests include free-space and wired optical communications, digital communications algorithms, and electronic and photonic implementation of coding and communication algorithms.

Dr. Hranilovic served as Cochair of the IEEE Communications Society, Toronto Chapter from 2000 to 2003.

Frank R. Kschischang (S'83–M'91–SM'00–F'06) received the B.A.Sc. (Honors) degree from the University of British Columbia, Vancouver, BC, Canada, in 1985, and the M.A.Sc. and Ph.D. degrees from the University of Toronto, Toronto, ON, Canada, in 1988 and 1991, respectively, all in electrical engineering.

During 1997–1998, he spent a sabbatical year as a Visiting Scientist at the Massachusetts Institute of Technology, Cambridge. Currently, he is a Professor and Canada Research Chair in the Department of Electrical and Computer Engineering, University of Toronto, where he has been a Faculty Member since 1991. His research interests include coding techniques, primarily on soft-decision decoding algorithms, trellis structure of codes, codes defined on graphs, and iterative decoders.

Dr. Kschischang served as Associate Editor for Coding Theory of the IEEE TRANSACTIONS ON INFORMATION THEORY from 1997 to 2000 and also served as the Technical Program Cochair for the 2004 IEEE International Symposium on Information Theory, held in Chicago, IL. He is a recipient of the Ontario Premier's Research Excellence Award. He is now a Fellow of the IEEE since January 2006.